1 **Enterotoxigenic *Escherichia coli* display a distinct growth**

2 **phase before entry into stationary phase with shifts in**

3 **tryptophan- fucose- and putrescine metabolism and**

4 **degradation of neurotransmitter precursors.**

5

6

7 **Running title:** Transcriptome and metabolome of ETEC during growth

8

9 Enrique Joffré[1]*, Xue Xiao[2], Mário S. P. Correia[3], Intawat Nookaew[4], Samantha

10 Sasse[3], Daniel Globisch[3], Baoli Zhu[2] and Åsa Sjöling[1]

11

12 [1] Department of Microbiology, Tumor and Cell Biology, Karolinska Institute, Stockholm,

13 Biomedicum A8, 17165, Stockholm, Sweden

14

15 [2] CAS Key Laboratory of Pathogenic Microbiology & Immunology, Institute of Microbiology,

16 Chinese Academy of Sciences, Beijing, 100101, PR China

17

18 [3] Department of Chemistry - BMC, Science for Life Laboratory, Uppsala University, Box 599,

19 SE-75124 Uppsala, Sweden.

20

21 [4] Department of Biomedical Informatics, College of Medicine, University of Arkansas for

22 Medical Sciences, Little Rock, Arkansas, 72205, USA

23

24 *Author correspondence

25 Enrique Joffré

26 Department of Microbiology, Tumor and Cell Biology, Karolinska Institute,

27 Stockholm, Biomedicum A8, S-17165, Stockholm, Sweden.

28 Enrique.joffre@ki.se

29

30 **Keywords:** ETEC, transcriptomics, metabolomics, diarrheal pathogen, growth

31 phases, *E. coli*, transient growth phase, neurotransmitter precursors

32

33

Abstract

Enterotoxigenic *Escherichia coli* (ETEC) is a major cause of diarrhea in children and adults in endemic areas. Gene regulation of ETEC during growth *in vitro* and *in vivo* needs to be further evaluated, and here we describe the full transcriptome and metabolome of ETEC during growth from mid-logarithmic growth to stationary phase in rich medium (LB medium). We identified specific genes and pathways subjected to rapid transient alterations in gene expression and metabolite production during the transition between logarithmic to stationary growth. The transient phase during late exponential growth is different from the subsequent induction of stationary phase-induced genes, including stress and survival responses as described earlier. The transient phase was characterized by the repression of genes and metabolites involved in organic substance transport. Genes involved in fucose and putrescine metabolism were upregulated, and genes involved in iron transport were repressed. Expression of toxins and colonization factors were not changed, suggesting retained virulence. Metabolomic analyses showed that the transient phase was characterized by a drop of intracellular amino acids, e.g., L-tyrosine, L-tryptophan, L-phenylalanine, L-leucine, and L-glutamic acid, followed by increased levels at induction of stationary phase. A pathway enrichment analysis of the entire transcriptome and metabolome showed activation of pathways involved in the degradation of neurotransmitters aminobutyrate (GABA) and precursors of 5-hydroxytryptamine (serotonin). This work provides a comprehensive framework for further studies on transcriptional and metabolic regulation in pathogenic *E. coli.*

Importance

We show that *E. coli,* exemplified by the pathogenic subspecies enterotoxigenic *E. coli* (ETEC), undergoes a stepwise transcriptional and metabolic transition into the stationary phase. At a specific entry point, *E. coli* induces activation and repression of specific pathways. This leads to a rapid decrease of intracellular levels of L-tyrosine, L-tryptophan, L-phenylalanine, L-leucine, and L-glutamic acid due to metabolism into secondary compounds. The resulting metabolic activity leads to an intense but short peak of indole production, suggesting that this is the previously described "indole peak," rapid decrease of intermediate molecules of bacterial neurotransmitters, increased putrescine and fucose uptake, increased glutathione levels, and decreased iron

67 uptake. This specific transient shift in gene expression and metabolomics is short-lived

68 and disappears when bacteria enter the stationary phase. We suggest it mainly prepares

69 bacteria for ceased growth, but the pathways involved suggest that this transient phase

70 substantially influences survival and virulence.

71

72

73

74

75

76

77

78

79

80

81

82

83

84

85

86

87

88

89

90

91

92

93

94

95

Background

96

97   *Escherichia coli* is a facultative anaerobic gram-negative bacterium that normally

98   inhabits the intestines of mammals and reptiles as a commensal bacterium. Pathogenic

99   *E. coli* have acquired extrachromosomal genetic properties that enable them to colonize

100   and adhere to the epithelium, thereby delivering toxins or virulence factors that harm

101   the host [1]. The virulence factors can either be located on plasmids or inserted in the

102   chromosomes as pathogenicity islands, and pathogenic *E. coli* can be found in most *E.*

103   *coli* phylogroups [2-4]. Enterotoxigenic *Escherichia coli* (ETEC) is characterized by

104   the production of the heat-labile toxin (LT) and/or the heat-stable toxin (ST). In most

105   cases, each bacterium expresses one to three colonization factors that mediate adhesion

106   to the epithelium in the small intestine [5, 6]. The toxins and colonization factors of

107   ETEC are mainly encoded on extrachromosomal plasmids that have been acquired by

108   horizontal transfer to ancestral commensal *E. coli*. Successful combinations of host and

109   plasmid may lead to global transmission of virulent clones with optimal colonization

110   and survival abilities [2, 4].

111

112   The molecular events that govern the virulence of ETEC are less well characterized

113   than several other intestinal pathogenic *E. coli*. Studies on ETEC have so far focused

114   on a few global regulators such as Crp, H-NS, and members of the AraC family such

115   as Rns and CsvR that were shown to regulate the toxins and/or CFs [7-11]. However,

116   virulence factors are not only the expression of toxins or colonization factors but can

117   also be expanded to involve the ability to persist host-induced stress or to facilitate

118   spreading or colonization ability. Studies using real-time PCR, microarrays, and RNA-

119   Seq have recently begun to elucidate the global and/or specific transcriptional

120   regulation in ETEC in response to host environmental factors such as bile and glucose

121   and adhesion to epithelial cells [8, 11-15].

122

123   In this study, we explored the transcriptional and metabolomic profile of two ETEC

124   clinical isolates belonging to a globally spread linage during growth from logarithmic

125   cell division to early stationary phase to elucidate the effect of growth on transcriptomic

126   profile and virulence gene regulation. We used a multi-omics approach including RNA-

127   seq and mass spectrometric global metabolomics techniques to analyze the global

128 regulation and provide a framework of *E. coli* genes, transcription factors, and analysis

129 of metabolites involved in different growth phases in Luria Bertani medium.

130

131 **Results**
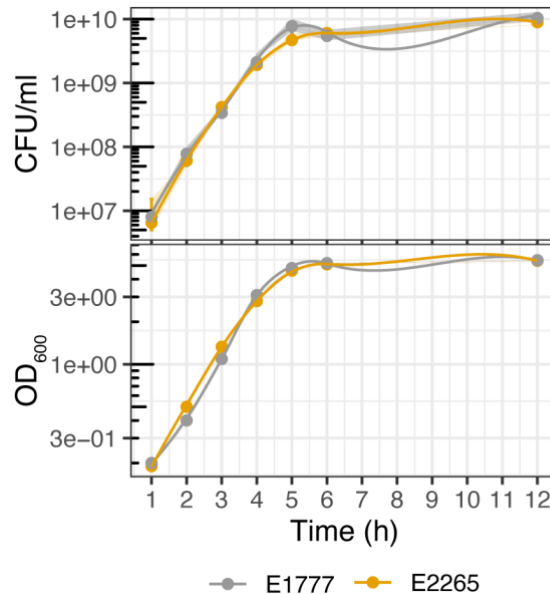
132

133 **Figure 1.** Growth curve of ETEC strains. Total bacterial counts in colony-forming units (CFU/ml) and

134 optic density (OD_{600}) of the ETEC strains E2265 and E1777 in LB media. Samples were measured every

135 hour for 12 hours.

136

137 **Expression profiling of two ETEC revealed characteristic transcriptional patterns**

138 **during transition from log phase to early stationary phase**

139 To profile the ETEC transcriptome during bacterial growth transition from mid-

140 exponential to early stationary phase, we performed RNA-seq analysis on RNA isolated

141 from two clinical isolates of ETEC (E1777 and E2265) grown in LB media. We

142 sequenced the transcripts expressed after 3, 4 and 5 hours of growth corresponding to

143 mid-log phase (3h, OD_{600} = 1.1-1.3), late log phase (4h, OD_{600} = 2.8-3.1) and early

144 stationary phase (5h, OD_{600} = 4.6-4.8) (Figure 1).

145

146 The two strains express LT STh, CS5+CS6, and belong to the globally distributed L5

147 ETEC lineage [4]. The time points were chosen to reflect the transition from active

148 growth to carbon and nutrient starvation, an environment that enteropathogens face in

149 the human gut and growth in LB [16]. First, Illumina sequence reads were assembled

150 and assigned as unigene sequences, translated, and compared to protein databases for

151 annotation. As a result, a total of 4166 unigenes with expression in at least one sample

152   were detected. Next, in order to identify the differentially expressed genes shared by

153   both isolates E2265 and E1777 and display the dynamic of the transcriptome during the

154   transition from the log phase (3h) to the early stationary phase (5h), we performed a

155   differential gene expression analysis by DESeq with a fold-change cutoff of 4 (Log2

156   >2) and p-value < 0.001. Overall, 617 genes (S Table 1, S Table 2) showed a significant

157   change (up/down) in at least one-time point, and these results were displayed and

158   clustered in a heatmap in Figure 2. The following comparisons, 3 h *vs.* 4 h and 3 h *vs.*

159   5 h resulted in a number of 486 (257 upregulated and 229 downregulated) and 392 (209

160   upregulated and 183 downregulated) differently expressed genes (DEG), respectively

161   (S Table 2). Thus, a total of 495 filtrated differentially expressed genes (DEG) in at

162   least one condition in both bacterial transcriptomes were included to perform the *K*-

163   means clustering analysis of the DEG heatmap (Figure 2 a; S Table 3) resulting in four

164   clusters of specific gene expression patterns (Cluster I-IV). In parallel, the Short Time-

165   series Expression Miner (STEM) clustering method [17] was performed using the same

166   dataset to identify differential gene expression patterns shared among genes with

167   similar dynamics in transcriptional changes over time (S Figure 1).

168   Thus, STEM (Figure 2 b and S Figure 1) identified eight temporal expression profiles,

169   of which four enclosed the majority of the genes, of which three (labeled in red, green,

170   and blue) showed a statistically significant ($p < 0.05$) higher number of genes assigned

171   using a permutation test. Both methods resulted in four distinctive temporal dynamics

172   of the transcriptome in response to the transition from log to early stationary phase (S

173   Table 4). In summary, clusters 1 and II were the largest, enclosing 166 and 110 genes,

174   respectively. Cluster I showed a decreasing expression towards the entry to the

175   stationary phase (3 h – 4 h – 5 h), while cluster III showed the opposite trend.

176   Interestingly, clusters II and IV included 19 and 74 genes, respectively, with a

177   significant transient down or up-regulation at 4 hours compared to 3 and 5 hours. Thus,

178   the data indicate that a specific transient phase in gene regulation occurs after 4 hours

179   and OD_{600} around 3 when ETEC enters the late log phase and starts transit into the

180   stationary phase.

181

182   In order to gain biological insights from the temporal transcriptomic dynamics, we

183   performed gene ontology (GO) enrichment analysis for biological processes and

184   metabolic pathways of the significantly expressed genes from each cluster (Figure 2 c;

185   S Table 5). Significant gene enrichment (FDR < 0.05) of cluster I indicated a notorious

186   downregulation of genes involved in the *de novo* purine biosynthesis pathways such as

187   'de novo' IMP biosynthetic processes as well as nitrogen metabolic pathways, and

188   protein targeting (intracellular protein transport) when growth slowed down upon entry

189   to late log phase and early stationary phase. In contrast, cluster III, which represents a

190   progressive transcriptional gene activation towards the stationary phase, was

191   significantly enriched in glyoxylate metabolism, TCA cycle, carboxylic acid metabolic

192   processes, aerobic respiration, and small molecule metabolism. Organic substance

193   transport, which involves the movement of organic substances that contains carbon in,

194   out, or within a cell, was solely identified as the most enriched biological process

195   among genes of cluster IV. No significant enrichment was identified for Cluster II.

196   Even though Clusters II and IV represent a minor proportion of the DEG dataset, they

197   exhibited an interesting transient transcriptional response prior to switching into the

198   stationary phase.
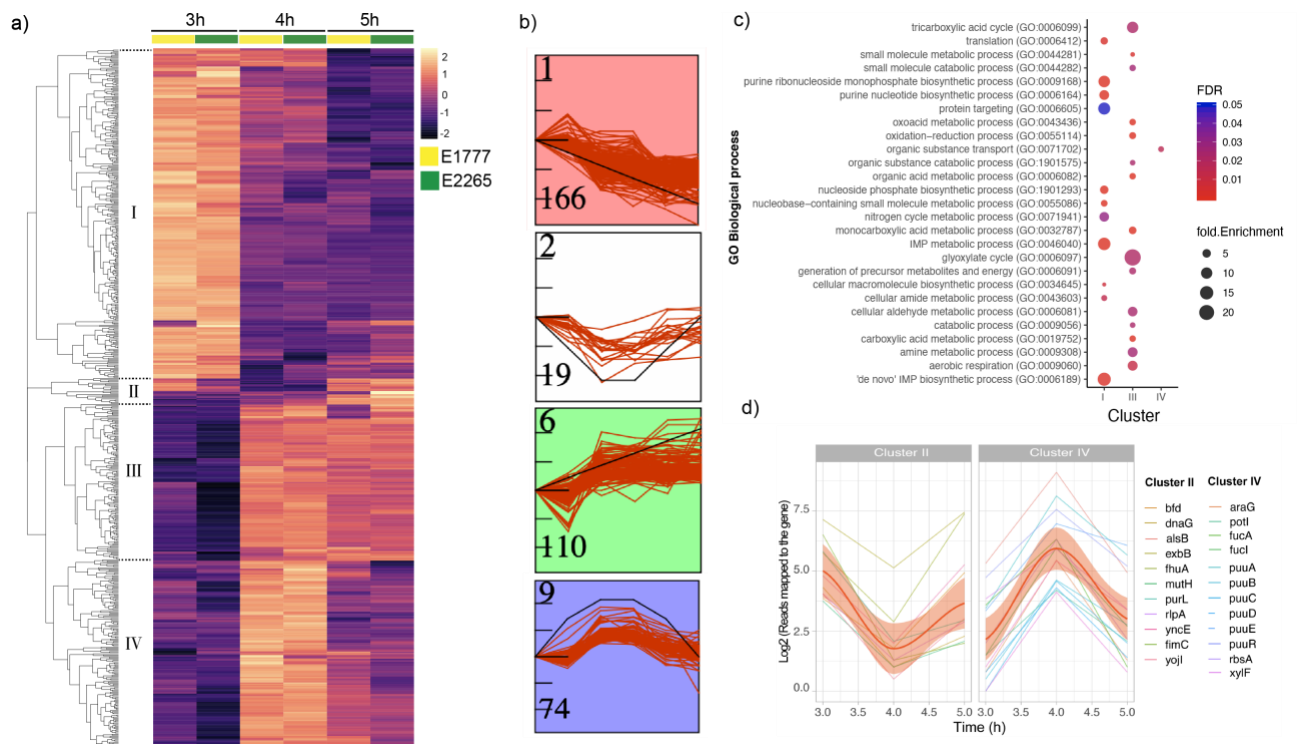
199

200   **Figure 2. Transcriptomic response of ETEC during bacterial growth transition from mid-**
201   **exponential to early stationary phase**. A) Heatmap of the differential expressions of the two strains
202   E1777 and E2265 after 3, 4, and 5 hours of growth in LB medium. K-*mers* analysis indicated 4 main
203   clusters (I-IV). B) STEM analysis identifying the most common patterns of gene expression. C) GO
204   Biological enrichment analysis of significant genes per cluster and fold enrichment. D) Set of genes with
205   transient up or down-regulation.

206

Transient transcriptomic activation of putrescine and fucose utilization and reduction of iron transport prior to entry into stationary phase.

The next step is to increase our understanding of the biological role of the transiently altered genes (4 hours of growth at the beginning of the stationary phase) identified in clusters II and IV. Reads mapped to the gene of each temporal gene expression were plotted in Figure 2d. The trendline confirmed the down (cluster II) and up (cluster IV) regulation of these genes during the transient shift to stationary phase. Among the activated genes at 4 h, we identified an overrepresentation of genes from the fuc operon, *i.e.*, *fucI* (L-fucose isomerase) and *fucA* (L-fucose 1-phosphate aldolase) and *fucU* (L-fucus mutarotase) with an approximately 6-fold increase in expression. Another set of genes involved in the exploitation of alternative nutrient sources was the putrescine pathway. Like the fucose operon, the Puu-operon (putrescine utilization pathway) genes that degrade putrescine to GABA via γ-glutamylated intermediates were highly activated at 4 h. Genes involved in the putrescine uptake system, *i.e.*, *potI* and *ydcU* showed the same pattern. Another gene included in this cluster was *tnaA*, which encodes tryptophanase, responsible for indole production from L-tryptophan. Its expression was activated 20-fold at 4 h compared to the mid-log growth phase at 3 h and reduced 6-fold at 5h (S Table 3). In addition, increased expression of the fad-operon (*fadH, FadM*) and the *dpp*-operon in charge of dipeptide transport were evident. Downregulation of genes in cluster II included *exbB* and *fhuA* involved in siderophore-mediated iron transport, *yncE*, a DNA binding protein involved in iron metabolism, and *bfd* bacterioferritin-associated ferredoxin; hence cluster II suggests that a rapid downregulation of genes involved in iron metabolism occurs transiently before entry into early stationary phase.

Expression of ETEC virulence factors is slightly higher during exponential growth

Both strains analyzed in this study expressed genes encoding the enterotoxins: *eltAB* (LT) and *estA* (STh), and colonization factor operons: *csfABCDEF* (CS5) and *cssABCD* (CS6) [18]. The transcriptome data showed that *eltAB* expression was higher than *estA* at all three-time points. In comparison with *estA* expression, *eltAB* was 3-4-fold higher at 3 hours and 2-4-fold and 2-fold at 4 and 5 hours, respectively. Expression of *eltAB* and the CS5 encoding *cfs*-operon, *estA,* and the CS6 had a trend of gradual downregulation over time (S Table 4). The expression patterns were similar between

240   the strains. Although the expression levels were not significantly changed in this study,

241   the findings are confirmed by our previous work [8]. Genome analysis showed that both

242   strains also express additional virulence genes: *cexE, clyA, eatA, ecpA,* and *fimH* [18].

243   These genes were not significantly changed.

244

245   **Global view of the intracellular and secreted metabolome of ETEC growth phases**

246   Since our transcriptomic data provided a framework of how metabolic pathways were

247   altered during the transition from freely available nutrients to a more restricted

248   environment, we wanted to characterize the impact of nutrient depletion on the bacterial

249   metabolome. We collected pellets (intracellular metabolites) and supernatants (secreted

250   metabolites) of E2265 and E1777 bacteria at 3, 4, and 5 hours of growth in LB broth

251   medium and performed a nontargeted GC-MS-based metabolomics approach.

252   Approximately 2000 putative intracellular and secreted metabolites were detected in

253   both isolates, of which 288 metabolites were successfully identified (S Table 6).

254   Principal component analysis (PCA) (Figure 3a) of all samples revealed a profound

255   clustering of samples from the intracellular and secreted metabolomes. The analysis

256   also indicated that the intracellular metabolomes of both E2265 and E1777 are more

257   similar than their respective secreted metabolome. The PCA did not show any variation

258   between metabolomes of the strains per time point (Figure 3a); however, the

259   hierarchical clustering heatmap showed changes in the abundance of several

260   metabolites along with the time points (S Figure 2).

261

262   *Intracellular and secreted metabolome show unique metabolomic shifts*

263   Since we are interested in studying the differences in the metabolome during bacterial

264   growth transition mid-exponential to early stationary phase, we used multiple t-tests to

265   compare the metabolite abundance between two time points, *i.e.,* 3 h versus 4 h or 3 h

266   versus 5 h (S Table 7, S Table 8). The threshold for significant changes was $|\log_2$ fold

267   change $> \log_2 2$; Padj < 0.05). As shown in Table 1, Figure 3 b, and S Figure 3, 35

268   metabolites significantly changed in their intracellular and/or extracellular

269   concentration at any time point. Specifically, 20 intracellular and 12 secreted

270   metabolites were significantly altered.

271   To characterize the chemical diversity of the intracellular and secreted ETEC

272   metabolomes and further explore the metabolic changes between the intracellular and

273   secreted ETEC metabolomes across the time points, the significant metabolites were

274   classified according to chemical classes (Human Metabolome DB; www.hmdb.ca) and

275   a hierarchical clustering heatmap based on the metabolite relative abundances was

276   generated. Ten and five metabolite classes were included in the intracellular and

277   secreted metabolome, respectively. The most common class of metabolites were amino

278   acids and peptides, as well as downstream catabolism metabolites. The metabolic

279   profile changes illustrated in the heatmap of Figure 3c indicated remarkable differences

280   in the metabolite abundance between ETEC metabolomes and some differences in the

281   metabolic profile between ETEC strains. For instance, betaine and the fatty acid 5-

282   aminopectanoic acid were only detected in E2265, and the amino acid *N*-methyl-L-

283   glutamic acid only in E1777 (Figure 3c).

284
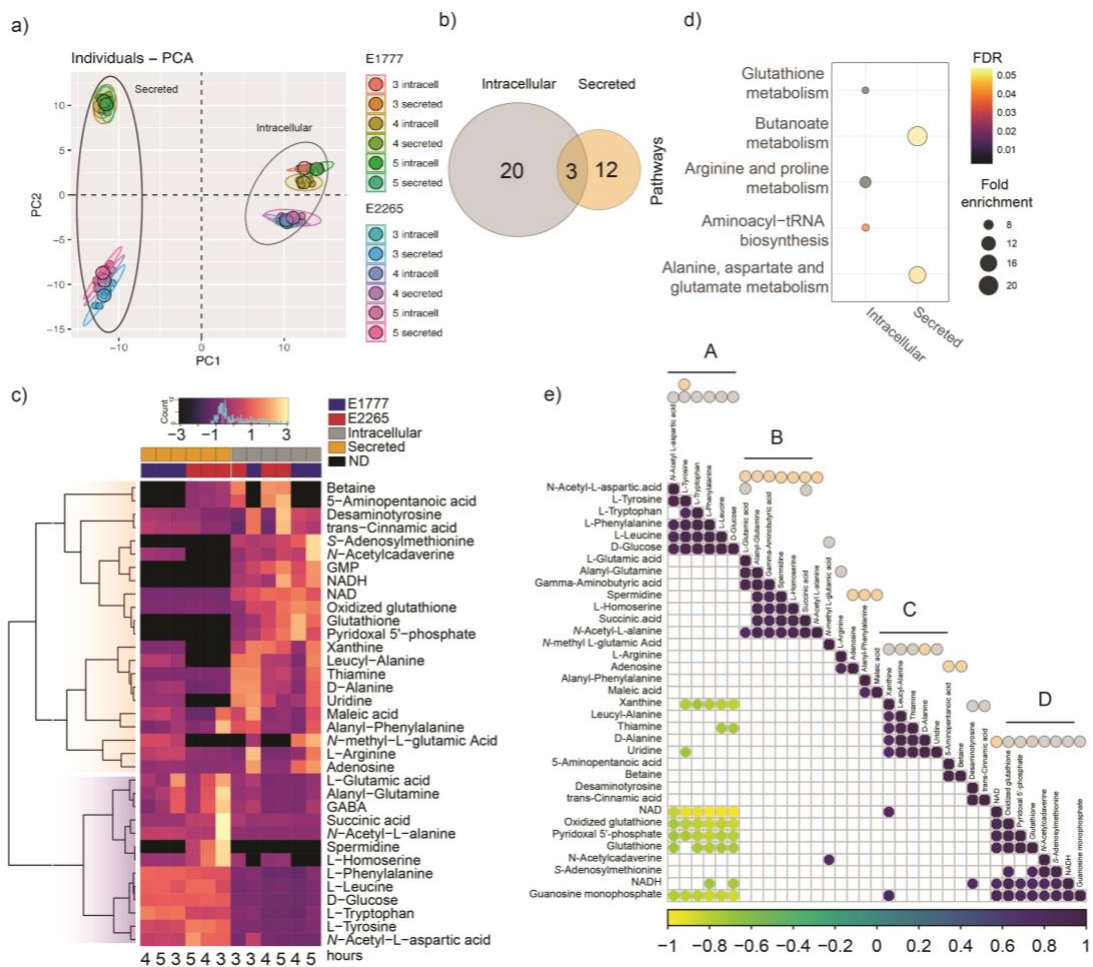
Figure 3. Intracellular and Secreted profile of the metabolic response to ETEC during bacterial growth transition from mid-exponential to early stationary phase. A) PCA plot generated from all metabolites of different samples. B) Venn diagrams of number of significant (p < 0.01 -2 > Log2Foldchange <2) found in the bacteria (intracellular) or medium (secreted). C) Heatmap representation of the 35 differentially changed metabolites at any time point. D) Pathway enrichment analysis of the intracellular and secreted significant metabolites. Non-significant pathways were colored gray. E) Metabolite-metabolite correlation analysis shows positive correlations in dark purple and

292 negative correlations in yellow. Secreted and intracellular metabolites were marked with orange and gray

293 dots, respectively.

294 Two main clusters of metabolite abundance patterns were identified: the first cluster

295 included a diverse set of metabolites with higher intracellular concentrations or absence

296 of secretion. For instance, *S*-adenosylmethionine, *N*-acetylcadaverine, GMP, NADH,

297 glutathione, and pyridoxal 5´-phosphate (PLP, known as the catalytically active form

298 of vitamin B_6) were not secreted at any time point by the two strains.

299

300 In the second cluster with higher levels of secreted metabolites than intracellular levels,

301 we found most of the amino acids identified in this dataset and glucose and succinic

302 acid. The amine spermidine was only detected in the E2265 supernatant, whereas the

303 amino acid L-homoserine was secreted at higher levels by E2265 than E1777, where

304 the metabolite was absent intracellularly (Figure 3c). Again, these data indicated that

305 although both ETEC strains are genetically very closely related, their physiology could

306 vary. The clustering patterns of samples per time point also confirmed significant

307 differences in metabolites abundance over time.

308

309 **Table 1. Summary of significantly altered intracellular and secreted metabolites of ETEC.**

310 Metabolites were classified based on the biochemical structure and in which metabolic pathways play a

311 role. Metabolite abundance is presented in fold change against 3 h. Values in bold represent $-2 >$

312 Log2Foldchange < 2 and underlined were statistically significant Padj < 0.05.

| Metabolite | Classification | HMDB ID | Intracellular | | | | Secreted | | | |
| | | | E1777 | | E2265 | | E1777 | | E2265 | |
			3h v 4h	3h v 5h	3h v 4h	3h v 5h	3h v 4h	3h v 5h	3h v 4h	3h v 5h
L-Glutamic acid	Amino acids and peptides	HMDB0000148	-2,24	-0,73	-1,76	-1,15	-1,59	-2,19	-0,87	-2,46
L-Tyrosine	Amino acids and peptides	HMDB0000158	-2,47	-0,11	-1,58	-0,99	-0,05	-0,15	0,21	0,25
Succinic acid	TCA acids	HMDB0000254	-3,37	-0,36	-2,01	-2,26	-0,51	-0,43	-2,43	-2,47
L-Arginine	Amino acids and peptides	HMDB0000517	-3,09	-0,48	-2,37	-1,79	-0,26	-0,03	0,15	0,33
L-Leucine	Amino acids and peptides	HMDB0000687	-2,44	-0,10	-0,41	0,27	0,19	0,21	0,43	0,45
L-Phenylalanine	Amino acids and peptides	HMDB0000159	-2,13	-0,03	-1,27	-0,79	0,04	-0,02	0,01	0,09
L-Tryptophan	Amino acids and peptides	HMDB0000929	-2,76	-0,04	-1,48	-1,12	0,11	-0,04	-0,10	-0,06
N-Acetyl-L-aspartic acid	Amino acids and peptides	HMDB0000812	-3,04	-3,30	0,59	-0,17	0,01	0,12	0,02	0,43
S-Adenosylmethionine	Glycosyl compounds	HMDB0001185	1,46	2,50	-0,05	0,49	0,00	0,00	0,00	0,00
D-Glucose	Monosaccharides	HMDB0000122	-3,27	-0,35	-1,94	-1,40	-0,03	0,01	0,07	0,02
Glutathione	Amino acids and peptides	HMDB0000125	3,02	2,32	3,56	4,27	0,00	0,00	0,00	0,00
Oxidized glutathione	Amino acids and peptides	HMDB0003337	0,87	0,71	1,69	2,39	0,40	0,48	1,17	1,29
GMP	Purines	HMDB0001397	0,23	1,11	1,60	2,13	0,00	0,00	0,00	0,00
Xanthine	Purines	HMDB0000292	-2,86	-0,03	1,14	0,76	0,06	0,11	0	0
N-methyl-L-glutamic Acid	Amino acids and peptides	HMDB0062660	2,02	2,48	0,00	0,00	0,63	0,58	0,00	0,00
NAD	Nicotinamides	HMDB0000902	0,48	-0,05	0,69	0,62	0,01	1,14	3,17	2,59
Pyridoxal 5'-phosphate	Pyridine carboxaldehydes	HMDB0001491	2,21	1,06	2,71	3,33	0,00	0,00	0,00	0,00
Thiamine	Pyrimidines	HMDB0000235	-2,46	-0,23	-1,29	-0,99	0,07	0,06	0,09	0,08
trans-Cinnamic acid	Cinnamic acids	HMDB0000930	-0,52	-0,72	0,15	2,19	0,16	0,05	-0,03	0,28
Uridine	Pyrimidines	HMDB0000296	-2,02	-0,48	-0,91	-2,35	0,03	0,02	0,00	0,00
Leucyl-Alanine	Amino acids and peptides	HMDB0028922	-3,14	0,02	-1,21	-1,27	0,57	0,61	0	0
N-Acetylcadaverine	Carboxylic acids	HMDB0002284	0,30	2,63	1,25	3,11	1,68	0,76	0,00	0,00
Desaminotyrosine	Phenylpropanoids	HMDB0002199	-0,49	-0,64	0,31	2,50	0,29	0,17	0,01	0,39
5-Aminopentanoic acid	Fatty acids	HMDB0003355	0	0	0,71	1,10	0	0	-0,85	-2,35
Adenosine	Purines	HMDB0000050	-0,49	-0,03	-0,31	-0,82	-0,99	0,03	-2,51	-3,14
Alanyl-Phenylalanine	Amino acids and peptides	HMDB0028694	-4,19	-0,06	-2,01	-2,00	-2,57	-1,49	-3,32	-4,60
Betaine	Amino acids and peptides	HMDB0000043	0	0	0,17	0,09	0	0	-1,28	-2,20
L-Homoserine	Amino acids and peptides	HMDB0000719	0	0	-2,70	-1,72	-0,29	0,00	-0,69	-2,20
Alanyl-Glutamine	Amino acids and peptides	HMDB0028685	-3,62	-0,26	-2,45	-2,43	-2,14	-1,12	-1,13	-3,02
D-Alanine	Amino acids and peptides	HMDB0001310	-2,79	-0,40	-1,24	-1,40	-0,32	-0,02	-1,19	-3,05
Spermidine	Amines	HMDB0001257	0	0	0	0	0	0	-0,81	-2,21
GABA	Amino acids and peptides	HMDB0000112	-2,35	-0,24	-1,77	-1,31	-2,90	-1,35	-0,82	-2,29
Maleic acid	Fatty acids	HMDB0000176	-2,52	-0,71	-1,20	-0,94	0,34	0,52	-3,32	-3,40
N-Acetyl-L-alanine	Amino acids and peptides	HMDB0000766	0	0	0	0	-0,07	0,02	-2,71	-2,69
NADH	Nicotinamides	HMDB0001487	0,86	1,66	-0,67	2,23	0,00	0,00	0,00	0,00

Pathway columns (color-coded): Aminoacyl-tRNA biosynthesis, Butanoate metabolism, Ala, Asp, and Glu metabolism, Arg and Pro metabolism, Glycolysis / Gluconeogenesis, Glutathione metabolism, Purine metabolism, Gly, Ser, and Thr metabolism, Methano metabolism, Nicotine/Nicotinamide metabolism, Vitamin B6 metabolism, Thiamine metabolism, phenylalanine metabolism, Pyrimidine metabolism, Muropeptide degradation, Peptidoglycan biosynthesis, NF.

A pathway enrichment analysis of significantly altered metabolites discovered general metabolic differences between both fractions. As is shown in Figure 3d, three KEGG pathways were differentially enriched (FDR < 0.05), and several other pathways were associated with the significant metabolites (Table 1). The intracellular metabolites with significant differences over the timepoints were enriched in the aminoacyl-tRNA biosynthesis pathway, including L-tyrosine, L-tryptophan, L-phenylalanine, L-leucine, and L-glutamic acid. These metabolites showed significantly decreased levels at 4 hours which were restored in E1777 at 5 hours but remained low in E2265. The intracellular glutathione levels increased 10-fold at 4 h compared to 3 h and remained high at 5 h. On the other hand, the pathways responsible for butanoate metabolism, alanine, aspartate, and glutamate metabolism were significantly enriched among secreted metabolites (Figure 4 c and S Table 9).

The butanoate metabolism pathway included the bacterial neurotransmitter GABA, L-glutamate, succinic acid, and maleic acid, and they were mainly secreted at 3 hours. These metabolites were found in lower concentrations in comparison with metabolites of the aminoacyl-tRNA biosynthesis pathway.

In order to investigate whether there were metabolite-metabolite correlations across the metabolomes, we calculated the Pearson correlation coefficients. We wanted to identify

333   the strongest correlations, and a total of 110 pairwise differentially significant

334   correlations ($P < 0.001$) were found, of which 74 were positive and 36 negative

335   metabolite-metabolite correlations. Most of these correlations were consistent with the

336   heatmap clustering; however, 4 sets of tightly correlated metabolite-metabolite

337   interaction were identified. As seen in Figure 3 e (S Table 10), all 4 grouped pairwise

338   metabolites positively correlated ($r < 0.8$). Most of the amino acid metabolites were

339   clustered in groups A and B, while the C and D groups included more diverse classes

340   of metabolites. The positive correlations emphasized their close biochemical

341   relatedness or overlapped roles among catabolic pathways. In contrast, metabolite-

342   metabolite correlations from A and D as well as xanthine, thiamine, and uridine from

343   the nucleotide metabolisms and A correlated negatively ($r < -0.6$).

344   Overall, the metabolome analysis of ETEC revealed distinctive differences in the

345   metabolic composition of the intracellular and external environment of the bacteria,

346   mainly characterized by the secretion or availability of large amounts of essential amino

347   acids, intermediates, and derived molecules such as GABA. In contrast, the intracellular

348   environment was characterized by a transient drop of amino acids at 4 hours of growth,

349   and glutathione redox-regulation was implicated in the adaptation to stationary phase

350   as reduced L-glutathione was increased 10-fold intracellularly.
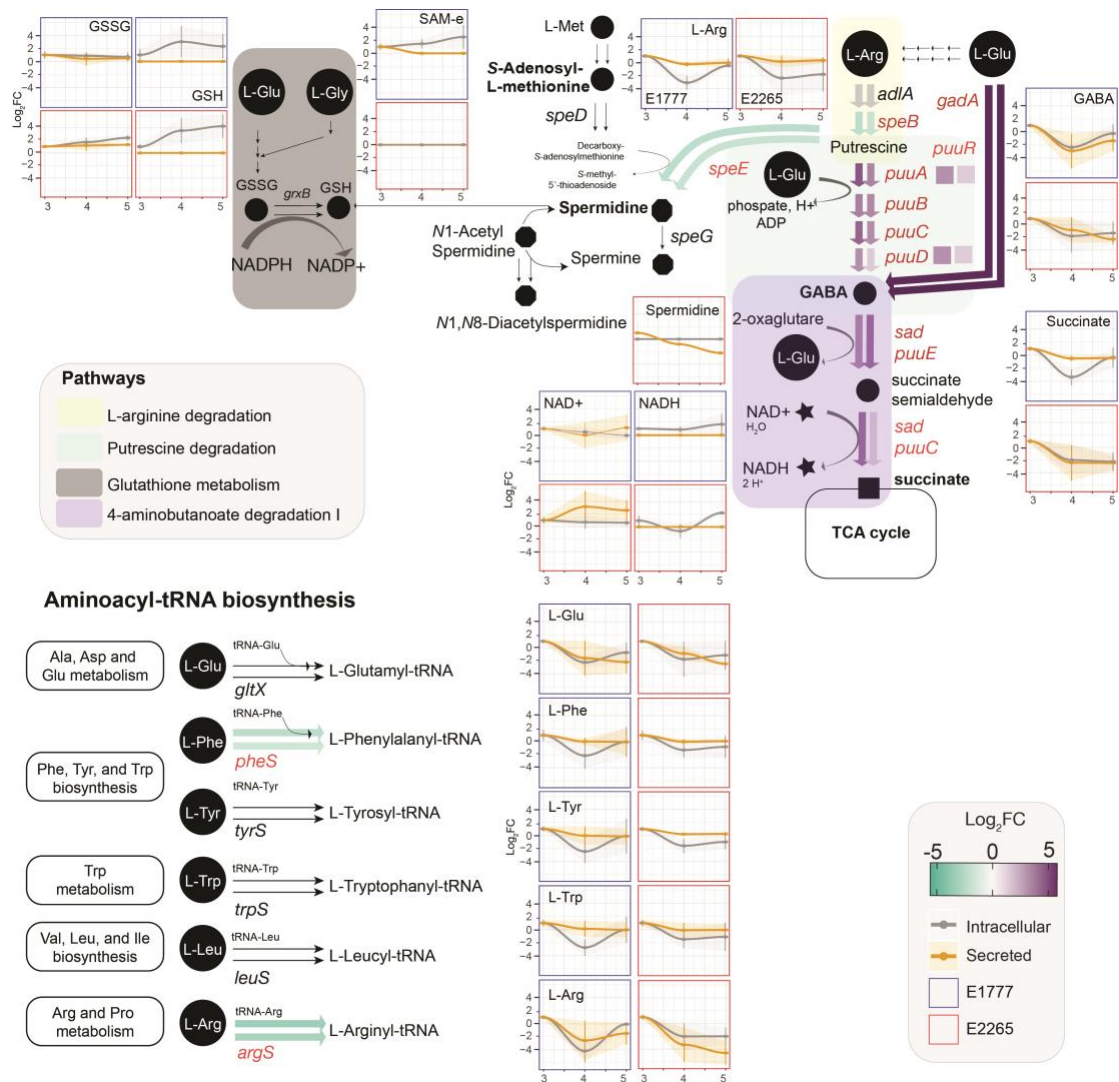
Figure 4. Transcriptomic and metabolic modulation of 4-butanoate degradation, related pathways, and Aminoacyl-tRNA biosynthesis of ETEC during growth. Circles are metabolites, and arrows are reactions. Verified metabolites are labeled in bold (S Table 12). The color of the width arrows indicates the levels of gene expression represented in the fold-change. The first and second arrows represent the DEG between 3 vs. 4 h and 3 vs. 5h. Data of the concentration of significant metabolites are represented in the serial charts. The metabolite concentration is adjusted to 3 h, and the data is presented in fold-change±SD.

Transcriptome and metabolome integration

Next, we combined the significant data from the transcriptomic analysis and metabolomics and mapped it into super pathways, including L-arginine, 4-aminobutanoate, and putrescine degradation (Figure 4 and S Table 11). This pathway uses L-arginine as a carbon source and degrades it to succinate for the TCA. Thus, at 4 hours, the concentrations of L-arginine, GABA -the intermediate molecule in the polyamine putrescine degradation, and succinate had a significant drop of its

367   concentration by 5-fold in both intracellular and extracellular environments remained

368   slightly lower towards the entry of the stationary phase. This was also consistent with

369   a significant transient upregulation of all *puu* operon genes at 4 hours. The expression

370   levels of *puuR*, the main repressor that regulates the intracellular putrescine

371   concentrations by repressing several genes of putrescine utilization and transport, had

372   the highest expression at 4 h. Glutamate and GABA are involved in the acid resistance

373   system 2 (AR2), which enteric bacteria use to survive acidic conditions [19]. A

374   significant increase in the expression of *gadA* and the glutamate decarboxylase at 4

375   hours suggests that bacteria initially convert L-glutamate to GABA, which is then

376   subsequently degraded since levels of glutamate, GABA, and succinate all rapidly

377   decrease intracellularly at 4 hours compared to 3 hours.

378

379   The degradation of putrescine can also form other polyamines such as spermidine and

380   spermine through L-methionine degradation. Spermine was found in large

381   concentrations at 3h and drastically decreased over time. The *S*-Adenosyl-L-

382   methionine, synthesized from the essential amino acid L-methionine was found in low

383   concentration at 4h and 5h (only in E1777) and subsequently converted by the

384   spermidine synthase (encoded by *speE*) to spermidine and later spermine, which was

385   found in lower concentration in the extracellular environment. Other acetylated

386   polyamines derived from spermidine such as N_1-acetylspermidine and N_1, N_8

387   diacetylspermidine were detected but not significantly changed over time. They

388   displayed mixed patterns with increasing concentrations in both supernatant and

389   intracellular fractions. Acetylation converts the polyamines to a physiologically inert

390   form to protect against polyamine toxicity and is mainly excreted from the cell. On the

391   other hand, spermidine can conjugate with thiol glutathione which plays a role in

392   detoxifying xenobiotics and reactive oxygen species. This thiol was detected at

393   increased concentrations over time intracellularly.

394

395   **Discussion**

396   Growth in Luria Bertani (LB) broth is commonly used to analyze bacterial properties.

397   Although most natural habitats of prokaryotes do not resemble the nutrients in LB, the

398   transition to more nutrient-depleted conditions, *i.e.,* the stationary phase when growth

399   ceases, is a common phenomenon in nature. We analyzed the transcriptome of two

400   ETEC strains during the transition from late exponential phase/early stationary phase

401   to stationary phase to get a comprehensive view of the regulatory and metabolic

402   pathways involved in ETEC and *E. coli* growth in LB. Our results indicated several

403   distinct steps during the transition into the stationary phase in support of previous

404   studies [20]. Specifically, we identified an interesting transient phase at $OD_{600} = 3$ at

405   the immediate onset of stationary phase characterized by decreased gene expression of

406   genes involved in iron uptake and more than 10-fold upregulation of operons involved

407   in, *e.g.,* dipeptide transport, fucose, and putrescine utilization and indole production.

408   Furthermore, integration of the transcriptome with metabolome analyses highlighted

409   the L-arginine, 4-aminobutanoate, and putrescine degradation pathways forcefully

410   induced at the onset of the stationary phase.

411

412   Our results suggested that the transient phase when ETEC/*E. coli* is preparing for

413   stationary phase is characterized by a temporal reduction in iron uptake. Interestingly,

414   a similar response has been reported in the transition phase between the log and

415   stationary phase for *Helicobacter pylori* [21], suggesting this phase alteration and its

416   characteristics occur in several bacterial species. Metal ions such as iron are essential

417   for bacteria but, at the same time, extremely toxic. Iron ions in oxidation state II (ferrous

418   (Fe^{2+}) iron are more bioavailable than ferric (Fe^{3+}) ions in oxidation state III but more

419   toxic since they may form hydroxyl radicals through the Fenton reaction. Our results

420   demonstrated that, e.g., *fecA* and *fhuA* related to iron uptake and transport of ferrous

421   ion and ferric ion were transiently downregulated during entry into stationary phase.

422   This may have implications in ensuring iron homeostasis in an iron-deficient

423   environment such as the gastrointestinal tract [22-24].

424

425   Transcriptome analysis also indicated increased fucose metabolism at the onset of

426   stationary phase at 4h followed by down-regulated at 5h. Fucose is an abundant mucus-

427   derived metabolite in the intestine generated by commensal bacteria [25]. The most

428   common commensal bacterium in the gut is *Bacteroides thetaiotaomicron,* and some

429   *E. coli* can utilize fucose as a carbon source [26]. We confirmed that E2265 used in this

430   study could metabolize L-fucose in a phenotypic assay, but interestingly this trait was

431   not conserved over all ETEC lineages. Several studies have shown the important role

432   of fucose in virulence. For example, in *Salmonella* Typhimurium, *fucI* was significantly

433   upregulated one day after infection in germ-free mice colonized by *Bacteroides*

434   *thetatiotaomicron,* and the respective mutant had decreased competitiveness *in vivo*

435   [27]. Another example of fucose modulating the virulence is EHEC, which harbors a

436   pathogenicity island LEE containing a two-complement-system (TCS) capable of

437   sensing fucose and transcribing the pathogenicity island LEE [28]. In EHEC, it has also

438   been demonstrated that fucose is important for colonization, suggesting that bacterial

439   pathogens take advantage of using unexploited sugars by commensal bacteria [29].

440   Hence the induction of fucose utilization might promote colonization of the mucosa of

441   bacteria in the early stationary growth phase. The fact that E2265 belongs to the

442   commonly isolated and globally spread clonal lineage 5 [4] might implicate that fucose

443   metabolism is important for virulence in certain ETEC lineages.

444

445   Pathway enrichment analysis identified two significant pathways; degradation of

446   aminobutyrate (GABA) degradation and degradation of 5- hydroxytryptamine

447   (serotonin), to be significantly enriched in cluster III characterized by genes that

448   progressively increased during entry into stationary phase (Fig 2). Genes involved, *e.g.,*

449   *puuE*, *gabD, aldAB, feaB,* and *prr* increased their expression levels up to 10-fold at 4

450   hours compared to 3 hours and increased further in the last sampling point at 5 hours.

451

452   The aminobutyrate degradation pathway (Fig 4) is linked to L-arginine and putrescine

453   degradation pathways. Putrescine and its downstream metabolite spermidine are

454   polyamines present in the gut and introduced by food, microbial, or intestinal cell

455   metabolism [30]. They regulate cellular function in both prokaryotic and eukaryotic

456   cells. The transient phase was characterized by upregulation of the *puu*-regulon.

457   Putrescine is generated by decarboxylation of ornithine or decarboxylation of arginine

458   into agmatine. *E. coli* uses specific importers such as PotFGHI and YdcU, members of

459   the ATP-binding cassette (ABC) transporter family, and PuuP to take up putrescine

460   across the cell membrane. Once putrescine is imported, PuuA γ-glutamylates putrescine

461   resulting in a γ-glutamyl-γ-aminobutyraldehyde, which is oxidized by PuuB and

462   subsequently dehydrogenated by PuuC. Then, PuuD hydrolyzes the resultant γ-

463   glutamyl group, generating and releasing simultaneously γ-aminobutyrate (GABA) and

464   glutamate. PuuE deaminates GABA to succinic semialdehyde, which is oxidated by

465   GabD (which does not belong to the Puu operon) to produce succinic acid that goes to

466   the TCA metabolism [31-33].

467

468 In terms of virulence, polyamines, specifically, putrescine has been shown to be
469 actively involved. For instance, a mutant of *potD* in *Streptococcus pneumoniae*
470 displayed attenuated virulence. In *V. cholerae*, defective biofilm formation was
471 observed after deletion of the homologous genes of *E. coli potD*. On the contrary,
472 polyamines might prevent the colonization of the small intestine by *V. cholerae* since
473 high concentrations of polyamines disrupt pili-pili interaction during autoaggregation
474 [34]. In *Salmonella enterica* serovar Typhimurium, exogenous putrescine and
475 spermidine are sensed to prime intracellular survival and induce virulence [35].

477 Interestingly, the downstream metabolite of putrescine γ-aminobutyric acid (GABA) is
478 a well-known neurotransmitter used as food supplementation in animal husbandry to
479 reduce aggressive behavior and stress [36]. Supplementation of GABA also induces
480 sIgA secretion and increases IL-4 and IL-17 in piglets challenged with porcine ETEC
481 [37]. The AraC-like transcription factor GadX is an activator of the glutamate
482 decarboxylase *gadAB* that converts L-glutamate to GABA. GadX is also a repressor of
483 the transcription factor that activates the expression of adhesion factor bundle forming
484 pilus (*bfp*) and intimin in enteropathogenic *E. coli* [38, 39]. Hence factors that increase
485 GABA might also downregulate virulence factors, and the corresponding rapid
486 degradation of GABA at the transient phase could promote virulence and
487 downregulated immune responses to ETEC. We could, however, not see the
488 corresponding pattern in this study since adhesion factors CS5 and CS6 were not
489 changed. Previous studies on transcriptomes in ETEC have indicated that toxin and CF
490 genes are down-regulated upon binding to cells as well as influenced by bile salts
491 present in the small intestine [11, 40, 41]. We have also previously shown that *eltAB*
492 expression decreases from exponential to stationary growth phase [8].

494 Tryptophan is cleaved to indole, pyruvate, and NH_4^+ by the tryptophanase (TnaA)
495 enzyme expressed by certain bacteria, including *E. coli, Bacteroides* and
496 *Lactobacilli*. Indole is an extracellular signaling molecule well known for affecting
497 different aspects of bacterial physiology, including biofilm formation, in a
498 concentration-dependent manner [42-45]. Indole is also an interspecies signaling
499 molecule. In *E. coli,* the "indole peak" has been described in several studies as a short
500 window of time at entry into the stationary phase where intracellular levels of indole

501   rapidly peak and then decrease again [42]. We found strong induction of *tnaA*

502   expression at 4h compared to 3h and 5h and concomitant rapid decrease of intracellular

503   L-tryptophan at 4h, supporting that the transient phase identified in this study is the

504   same as the indole peak.

505

506   Tryptophan metabolism in the gut is important since tryptophan metabolites include

507   indole and neurotransmitters and immunomodulators, including serotonin, tryptamine,

508   and kynurenine. The synthesis of these latter molecules is performed in gut cells like

509   enterochromaffin cells from diet-derived tryptophan and constitutes an important part

510   of the gut-brain axis of neurotransmitters [46]. In this study, metabolomics identified

511   L-5-hydroxytryptophan (5-HTP), the precursor of serotonin (5-hydroxytryptamine),

512   and we also found L-kynurenine (Supplementary Table 6). To our knowledge, only one

513   other study reported that *E. coli* could produce the neurotransmitter serotonin [47]. We

514   performed an additional verification analysis (S Table 12) to search for serotonin in

515   ETEC but were not able to detect it in our samples.

516   This study supports that commensal and pathogenic bacteria can both degrade and

517   produce neurotransmitters and their intermediate molecules and hence ETEC infection

518   might interact with gut cell signaling and influence the gut-brain axis to a larger extent

519   than previously thought.

520

521   In summary, our data suggest that the entry into the stationary phase is a distinct growth

522   phase that might pose ETEC into a stage of increased survival, virulence, and host

523   competitiveness due to lack of need to sequester iron, retained virulence gene

524   expression, and capacity to compete with the commensal flora for host-derived carbon

525   and nitrogen sources such as fucose and putrescine. This study provides a framework

526   for further studies on ETEC gene regulation and comprehensive characterization of

527   transcriptional responses during the transition to the stationary phase that also applies

528   to other bacteria.

529

Materials and Methods

531   *Strains, growth conditions, and bacterial enumeration.*

532   The ETEC strains E1777 and E2265 (LT STh/CS5+CS6), both isolated from adult

533   patients with watery diarrhea in Dhaka Bangladesh in 2005 and 2006, respectively,

534 were used in this study [12, 48]. The whole-genome sequences of the two strains are

535 available [18], including a complete assembled chromosome and two plasmids of 142

536 and 78 kbp, respectively, for E2265 [11, 48]. Bacteria from frozen stock vials were

537 grown on blood plates, and 10 colonies were picked and grown under shaking

538 conditions in 10 ml of LB medium to $OD_{600} = 0.8$ (10^9 bacteria/ml) to be used as a

539 starting culture. The starting culture was diluted 100-fold in 20 ml LB medium in a 250

540 ml Erlenmeyer flask and grown aerated at 150 rpm rotation at 37 ℃. Samples for optical

541 density, colony-forming units (cfu), and RNA extraction and metabolomics were

542 withdrawn after 3, 4, and 5 hours. For bacterial enumeration, the track dilution method

543 was performed as described previously [49]. In brief, a 20 µl of bacterial culture was

544 collected every hour up to 6 h and overnight time point and subjected to ten-fold serial

545 dilution in a 96-well plate filled with 180 µl of phosphate-buffered saline (PBS) 1X. 10

546 µl from each dilution were spotted in a column onto LB agar plates, and the plate was

547 tipped onto its side to allow migration of the spots across the agar surface. This step

548 was performed in duplicate. LB plates were incubated overnight at 37°C, and cfu per

549 ml was quantified by multiplying the number of colonies of each tract by their

550 respective dilution factor and inoculated volume (0.01 ml).

551 For RNA extraction, bacterial samples from 3, 4, and 5 h time points were immediately

552 mixed with 2 x volume of RNAProtect® (Qiagen) using the manufacturer's protocol.

553 Samples were stored at -80°C until extraction.

554

555 *RNA preparation*

556 Total RNA was prepared from lysozyme and proteinase K lysed bacteria using the

557 RNeasy® Mini Kit (Qiagen, Hilden, Germany) and the instructions provided by the

558 manufacturer for RNA extraction from Gram-negative bacteria. An extra step to

559 remove contaminating DNA on-column was included using the RNase-Free DNase Set

560 (Qiagen). The integrity of the RNA and absence of contaminating DNA was checked

561 by agarose gel electrophoresis, and the RNA concentration was measured

562 spectrophotometrically using a NanoDrop® ND-1000 (NanoDrop Technologies,

563 Wilmington, DE). The RNA was carefully precipitated, washed, and shipped under

564 99.5% EtOH. The integrity, quality, and concentrations of the RNA were rechecked

565 upon arrival at the sequencing facility at Beijing Genome Institute (BGI), Shenzhen,

566 China, using an Agilent. The RIN values were above 9.8 for all samples.

567

568   *RNA-seq*

569   The RNA samples were depleted from rRNA by RiboZero, and Illumina libraries were

570   generated using the TruSeq protocol described by the manufacturer. The libraries were

571   sequenced using the Hi-Seq 200 using a read length of 100 bp. Reads were assembled

572   using the software SOAPdenovo (http://soap.genomics.org.cn/ soapdenovo.html).

573   CAP3 assembled all the unigenes from different samples to form a single set of non-

574   redundant unigenes. All unigene sequences were blasted against protein databases

575   using blastx (e-value<0.00001) in the following order: Nr SwissProt:KEGG:COG.

576   Unigene sequences with hits in the first or second database did not go to the next search

577   round against later databases. Then blast results were used to extract CDS from Unigene

578   sequences and translate them into peptide sequences. Blast results information was also

579   used to train ESTScan [50]. CDS of unigenes with no-hit in the blast were predicted by

580   ESTScan and then translated into peptide sequences.

581   Functional annotations of Unigenes included protein sequence similarity, KEGG

582   Pathway, COG, and Gene Ontology (GO) was performed. First, all-Unigene sequences

583   were searched against protein databases (Nr SwissProt KEGG COG) using blastx (e-

584   value<0.00001). Then, the Blast2GO program [51] was used to get GO annotations of

585   the Unigenes. After getting GO annotation for every Unigene, we used WEGO software

586   [52] to do GO functional classification for all Unigenes.

587   Each time point's differential expression was determined using the DESeq2 package

588   (v1.22.1) and R-3.6.0 [53]. The counts were normalized, and the fold change and the

589   log2 of the fold-change were calculated based on the following comparisons: control

590   (3 h) vs. 4 h and control vs. 5 h. Significant genes from each comparison and each strain

591   were filtrated using the following threshold: Padj < 0.05, log2Foldchange < -2 and

592   log2foldchange > 2. PCA and sample distance heatmaps were plotted to visualize the

593   cluster of groups and outliers. Heatmaps of differential genes were generated using the

594   R package *pheatmap* [54]. For temporal gene expression pattern analysis, the Short

595   time-series Expression miner (STEM) was applied as described by Ernst, Nau [17]. For

596   gene ontology (GO) enrichment analysis for biological processes and metabolic

597   pathways, PATHER Overrepresenaton Test (http://www.pantherdb.org/) [55] with an

598   FDR correction applied to all reported P values for the statistical tests.

599

600   ***Untargeted Metabolomics***

Bacterial sampling

The bacterial sampling for metabolomics was performed as described previously [56] with some modifications. A total of 4 ml of bacterial culture were collected and split into two sterile Eppendorf tubes to sample intracellular and secreted metabolites at every time point. In addition, another 100 µl were collected for measurement of the optical density and pH. For extracellular metabolites, 2 ml of bacterial culture was pelleted by centrifugation at 12,000 x *g* for 3 min a tabletop centrifuge, and the supernatants were carefully removed and transferred to a new sterile Eppendorf tube for snap-frizzing in liquid nitrogen. Snap frozen samples were stored at -80°C. The fast filtration method was applied for intracellular metabolites using a 3-place EZ-FitTM Manifold (Millipore®) connected to a single vacuum that supports simultaneous filtration of three samples. A sterile 22 mm diameter MF-Millipore® membrane filter with 0.45-µm pore size was placed onto each manifold, pre-washed with pre-warmed LB medium, and the vacuum set to 50 mbar. 2 ml of the bacterial culture were pipetted in the middle of the filter and subsequently perfused with 5 ml of pre-warmed washing buffer (M9 medium [Sigma-Aldrich] adjusted to pH 7.3) was perfused. Immediately after, the cell-loaded filter was removed and transferred to an Eppendorf tube for snap-freezing in liquid nitrogen. 2 ml aliquots of LB and M9 minimal medium (Sigma-Aldrich) were collected and span-frizzed and used as negative controls. All tubes were kept at -80°C and shipped in dry ice to the Science for Life Laboratory at Uppsala University for metabolite extraction and UPLC-MS analysis.

Metabolite Extraction

Supernatants were extracted by the addition of 4 mL of 60:40 ethanol: water solution. The mixture was kept at 78 °C for 3 min, with vigorous mixing every minute. The filters containing the bacterial pellet were transferred to a 4 ml solution and kept at 78 °C for 3 min, with vigorous mixing every minute. The samples were transferred to Eppendorf tubes on ice and centrifuged at 13500 rpm for 5 min, at 4 °C. The supernatant was collected and dried under vacuum on a Speedvac concentrator. The pellet was re-dissolved and injected onto the UPLC-MS system.

UPLC-MS Analysis

633   Ultra-high-performance liquid chromatography coupled to a mass spectrometer
634   (UPLC-MS) was used to identify metabolites, which differ between the three different
635   time points. Mass spectrometric analysis was performed on an Acquity UPLC system
636   connected to a Synapt G2 Q-TOF mass spectrometer, both from Waters Corporation
637   (Milford, MA, USA). The system was controlled using the MassLynx software package
638   v 4.1, also from Waters. The separation was performed on an Acquity UPLC® HSS T3
639   column (1.8 µm, 100×2.1 mm) from Waters Corporation. The mobile phase consisted
640   of 0.1% formic acid in MilliQ water (A) and 0.1% formic acid in LC-MS grade
641   methanol (B). The column temperature was 40 °C and the mobile phase gradient
642   applied was as follows: 0-2 min, 0% B; 2-15 min, 0-100 % B; 15-18 min, 100 % B; 18-
643   20 min, 100-0 % B; 20-25 min, 0 % B, with a flow rate of 0.3 ml/min.
644   The samples were introduced into the q-TOF using positive electrospray ionization.
645   The capillary voltage was set to 2.50 kV and the cone voltage was 40 V. The source
646   temperature was 100 °C, the cone gas flow 50 l/min, and the desolvation gas flow 600
647   l/h. The instrument was operated in MSE mode, the scan range was m/z = 50-1200, and
648   the scan time was 0.3 s. A solution of sodium formate (0.5 mM in 2-propanol: water,
649   90:10, v/v) was used to calibrate the instrument, and a solution of leucine-encephalin
650   (2 ng/µl in acetonitrile: 0.1% formic acid in the water, 50:50, v/v) was used for the lock
651   mass correction at an injection rate of 30 s.
652
653   *Data analysis*
654   The obtained UPLC-MS data comparing the different time points were analyzed using
655   the XCMS software package under R (version 3.3.0) to perform peak detection,
656   alignment, peak filling, and integration. The peaks were annotated by comparing their
657   m/z values to the exact molecular masses of all the online platform Metaboanalyst for
658   pathway analysis. The *Escherichia coli* K-12 MG1655 from the KEGG database was
659   used for metabolite identification. Confirmed metabolites were co-injected with the
660   bacterial samples for the highest level of confirmation. The structures for the
661   significantly altered metabolites were validated with authentic internal standards, as
662   detailed in Figure S12. PCA and heatmaps were performed in R software. The
663   metabolite-metabolite correlations were computed using the R function *rcorr* from the
664   Hmisc   package   (https://cran.r-project.org/web/packages/Hmisc/index.html).   A
665   multiple parametric statistic t-test was performed in GraphPad to compare the means

666 of two paired groups, *i.e.,* 3 h vs. 4 h, and multiple comparison corrections were applied

667 using the Holm-Šídák method. *P-value* < 0.05 was set as the threshold for significance.

668

678

679

680 # **References**

681

682 1. Nataro, J.P. and J.B. Kaper, *Diarrheagenic Escherichia coli.* Clin Microbiol Rev, 1998. **11**(1):
683 p. 142-201.
684 2. Turner, S.M., et al., *Phylogenetic Comparisons Reveal Multiple Acquisitions of the Toxin
685 Genes by Enterotoxigenic Escherichia coli Strains of Different Evolutionary Lineages.* Journal
686 of Clinical Microbiology, 2006. **44**(12): p. 4528-4536.
687 3. Hazen, T.H., et al., *Draft Genome Sequences of Three O157 Enteropathogenic Escherichia
688 coli Isolates.* Genome Announc, 2013. **1**(4).
689 4. von Mentzer, A., et al., *Identification of enterotoxigenic Escherichia coli (ETEC) clades with
690 long-term global distribution.* Nat Genet, 2014. **46**(12): p. 1321-6.
691 5. Gaastra, W. and A.M. Svennerholm, *Colonization factors of human enterotoxigenic
692 Escherichia coli (ETEC).* Trends Microbiol, 1996. **4**(11): p. 444-52.
693 6. Qadri, F., et al., *Enterotoxigenic Escherichia coli in developing countries: epidemiology,
694 microbiology, clinical features, treatment, and prevention.* Clin Microbiol Rev, 2005. **18**(3):
695 p. 465-83.
696 7. Bodero, M.D. and G.P. Munson, *Cyclic AMP Receptor Protein-Dependent Repression of
697 Heat-Labile Enterotoxin.* Infection and Immunity, 2009. **77**(2): p. 791-798.
698 8. Gonzales, L., et al., *Alkaline pH Is a signal for optimal production and secretion of the heat
699 labile toxin, LT in enterotoxigenic Escherichia coli (ETEC).* PLoS One, 2013. **8**(9): p. e74069.
700 9. Haycocks, J.R.J., et al., *The Molecular Basis for Control of ETEC Enterotoxin Expression in
701 Response to Environment and Host.* PLoS Pathogens, 2015. **11**(1): p. e1004605.
702 10. Hodson, C., et al., *Control of Virulence Gene Expression by the Master Regulator, CfaD, in
703 the Prototypical Enterotoxigenic Escherichia coli Strain, H10407.* Frontiers in Microbiology,
704 2017. **8**(1525).
705 11. Joffre, E., et al., *The bile salt glycocholate induces global changes in gene and protein
706 expression and activates virulence in enterotoxigenic Escherichia coli.* Scientific Reports,
707 2019. **9**(1): p. 108.
708 12. Nicklasson, M., et al., *Expression of colonization factor CS5 of enterotoxigenic Escherichia
709 coli (ETEC) is enhanced in vivo and by the bile component Na glycocholate hydrate.* PLoS
710 One, 2012. **7**(4): p. e35827.
711 13. Sahl, J.W., et al., *A comparative genomic analysis of diverse clonal types of enterotoxigenic
712 Escherichia coli reveals pathovar-specific conservation.* Infect Immun, 2011. **79**(2): p. 950-
713 60.

714   14.   Hazen, T.H., et al., *Genome and Functional Characterization of Colonization Factor Antigen*
715   *I- and CS6-Encoding Heat-Stable Enterotoxin-Only Enterotoxigenic <i>Escherichia coli</i>*
716   *Reveals Lineage and Geographic Variation.* mSystems, 2019. **4**(1): p. e00329-18.
717   15.   Crofts, A.A., et al., *Enterotoxigenic E. coli virulence gene regulation in human*
718   *infections.* Proceedings of the National Academy of Sciences, 2018. **115**(38): p. E8968-
719   E8976.
720   16.   Sezonov, G., D. Joseleau-Petit, and R. D'Ari, *Escherichia coli physiology in Luria-Bertani*
721   *broth.* J Bacteriol, 2007. **189**(23): p. 8746-9.
722   17.   Ernst, J., G.J. Nau, and Z. Bar-Joseph, *Clustering short time series gene expression data.*
723   Bioinformatics, 2005. **21 Suppl 1**: p. i159-68.
724   18.   Liu, F., et al., *Draft genomes of four enterotoxigenic Escherichia coli (ETEC) clinical isolates*
725   *from China and Bangladesh.* Gut Pathog, 2015. **7**: p. 10.
726   19.   Feehily, C. and K.A.G. Karatzas, *Role of glutamate metabolism in bacterial responses*
727   *towards acid and other stresses.* Journal of Applied Microbiology, 2013. **114**(1): p. 11-24.
728   20.   Martinez-Antonio, A., et al., *Regulatory design governing progression of population growth*
729   *phases in bacteria.* PLoS One, 2012. **7**(2): p. e30654.
730   21.   Thompson, L.J., et al., *Gene expression profiling of Helicobacter pylori reveals a growth-*
731   *phase-dependent switch in virulence gene expression.* Infect Immun, 2003. **71**(5): p. 2643-55.
732   22.   Holden, V.I. and M.A. Bachman, *Diverging roles of bacterial siderophores during infection.*
733   Metallomics, 2015.
734   23.   Andrews, S.C., A.K. Robinson, and F. Rodriguez-Quinones, *Bacterial iron homeostasis.*
735   FEMS Microbiol Rev, 2003. **27**(2-3): p. 215-37.
736   24.   Saha, R., et al., *Microbial siderophores: a mini review.* J Basic Microbiol, 2013. **53**(4): p.
737   303-17.
738   25.   Kamada, N., et al., *Control of pathogens and pathobionts by the gut microbiota.* Nat
739   Immunol, 2013. **14**(7): p. 685-90.
740   26.   Hooper, L.V., et al., *A molecular sensor that allows a gut commensal to control its nutrient*
741   *foundation in a competitive ecosystem.* Proc Natl Acad Sci U S A, 1999. **96**(17): p. 9833-8.
742   27.   Ng, K.M., et al., *Microbiota-liberated host sugars facilitate post-antibiotic expansion of*
743   *enteric pathogens.* Nature, 2013. **502**(7469): p. 96-9.
744   28.   Pacheco, A.R., et al., *Fucose sensing regulates bacterial intestinal colonization.* Nature, 2012.
745   **492**(7427): p. 113-7.
746   29.   Fabich, A.J., et al., *Comparison of carbon nutrition for pathogenic and commensal*
747   *Escherichia coli strains in the mouse intestine.* Infect Immun, 2008. **76**(3): p. 1143-52.
748   30.   Tofalo, R., S. Cocchi, and G. Suzzi, *Polyamines and Gut Microbiota.* Frontiers in nutrition,
749   2019. **6**: p. 16-16.
750   31.   Nemoto, N., et al., *Mechanism for regulation of the putrescine utilization pathway by the*
751   *transcription factor PuuR in Escherichia coli K-12.* J Bacteriol, 2012. **194**(13): p. 3437-47.
752   32.   Schneider, B.L., V.J. Hernandez, and L. Reitzer, *Putrescine catabolism is a metabolic*
753   *response to several stresses in Escherichia coli.* Mol Microbiol, 2013. **88**(3): p. 537-50.
754   33.   Kurihara, S., et al., *A novel putrescine utilization pathway involves gamma-glutamylated*
755   *intermediates of Escherichia coli K-12.* J Biol Chem, 2005. **280**(6): p. 4602-8.
756   34.   Goforth, J.B., N.E. Walter, and E. Karatan, *Effects of Polyamines on Vibrio cholerae*
757   *Virulence Properties.* PLoS ONE, 2013. **8**(4): p. e60765.
758   35.   Jelsbak, L., et al., *Polyamines Are Required for Virulence in <italic>Salmonella*
759   *enterica</italic> Serovar Typhimurium.* PLoS ONE, 2012. **7**(4): p. e36149.
760   36.   H., L.Y., et al., *Effect of γ-aminobutyric acid on growth performance, behavior and plasma*
761   *hormones in weaned pigs.* Canadian Journal of Animal Science, 2015. **95**(2): p. 165-171.
762   37.   Zhao, Y., et al., *Effects of GABA Supplementation on Intestinal SIgA Secretion and Gut*
763   *Microbiota in the Healthy and ETEC-Infected Weanling Piglets.* Mediators Inflamm, 2020.
764   **2020**: p. 7368483.
765   38.   Shin, S., et al., *An activator of glutamate decarboxylase genes regulates the expression of*
766   *enteropathogenic Escherichia coli virulence genes through control of the plasmid-encoded*
767   *regulator, Per.* Mol Microbiol, 2001. **41**(5): p. 1133-50.
768   39.   Braun, H.S., et al., *The GadX regulon affects virulence gene expression and adhesion of*
769   *porcine enteropathogenic Escherichia coli in vitro.* Vet Anim Sci, 2017. **3**: p. 10-17.
770   40.   Kansal, R., et al., *Transcriptional modulation of enterotoxigenic Escherichia coli virulence*
771   *genes in response to epithelial cell interactions.* Infect Immun, 2013. **81**(1): p. 259-70.

772   41.   Joffré, E., et al., *Identification of new heat-stable (STa) enterotoxin allele variants produced by human enterotoxigenic Escherichia coli (ETEC).* Int J Med Microbiol, 2016. **306**(7): p. 586-594.

775   42.   Gaimster, H., et al., *The indole pulse: a new perspective on indole signalling in Escherichia coli.* PLoS One, 2014. **9**(4): p. e93168.

777   43.   Bansal, T., et al., *The bacterial signal indole increases epithelial-cell tight-junction resistance and attenuates indicators of inflammation.* Proc Natl Acad Sci U S A, 2010. **107**(1): p. 228-33.

780   44.   Lee, J., A. Jayaraman, and T.K. Wood, *Indole is an inter-species biofilm signal mediated by SdiA.* BMC Microbiol, 2007. **7**: p. 42.

782   45.   Li, G. and K.D. Young, *Indole production by the tryptophanase TnaA in Escherichia coli is determined by the amount of exogenous tryptophan.* Microbiology, 2013. **159**(Pt 2): p. 402-10.

785   46.   O'Mahony, S.M., et al., *Serotonin, tryptophan metabolism and the brain-gut-microbiome axis.* Behav Brain Res, 2015. **277**: p. 32-48.

787   47.   Shishov, V.A., et al., *Amine neuromediators, their precursors, and oxidation products in the culture of Escherichia coli K-12.* Applied Biochemistry and Microbiology, 2009. **45**(5): p. 494-497.

790   48.   Begum, Y.A., et al., *In Situ Analyses Directly in Diarrheal Stool Reveal Large Variations in Bacterial Load and Active Toxin Expression of Enterotoxigenic Escherichiacoli and Vibrio cholerae.* mSphere, 2018. **3**(1).

793   49.   Jett, B.D., et al., *Simplified agar plate method for quantifying viable bacteria.* Biotechniques, 1997. **23**(4): p. 648-50.

795   50.   Iseli, C., C.V. Jongeneel, and P. Bucher, *ESTScan: a program for detecting, evaluating, and reconstructing potential coding regions in EST sequences.* Proc Int Conf Intell Syst Mol Biol, 1999: p. 138-48.

798   51.   Conesa, A., et al., *Blast2GO: a universal tool for annotation, visualization and analysis in functional genomics research.* Bioinformatics, 2005. **21**(18): p. 3674-6.

800   52.   Ye, J., et al., *WEGO: a web tool for plotting GO annotations.* Nucleic Acids Res, 2006. **34**(Web Server issue): p. W293-7.

802   53.   Love, M.I., W. Huber, and S. Anders, *Moderated estimation of fold change and dispersion for RNA-seq data with DESeq2.* Genome Biology, 2014. **15**(12): p. 550.

804   54.   Kolde, R., *pheatmap: Pretty Heatmaps. R package version 0.7. 7.* 2013.

805   55.   Mi, H. and P. Thomas, *PANTHER pathway: an ontology-based pathway database coupled with data analysis tools.* Methods in molecular biology (Clifton, N.J.), 2009. **563**: p. 123-140.

807   56.   Link, H., J.M. Buescher, and U. Sauer, *Chapter 5 - Targeted and quantitative metabolomics in bacteria*, in *Methods in Microbiology*, C. Harwood and A. Wipat, Editors. 2012, Academic Press. p. 127-150.
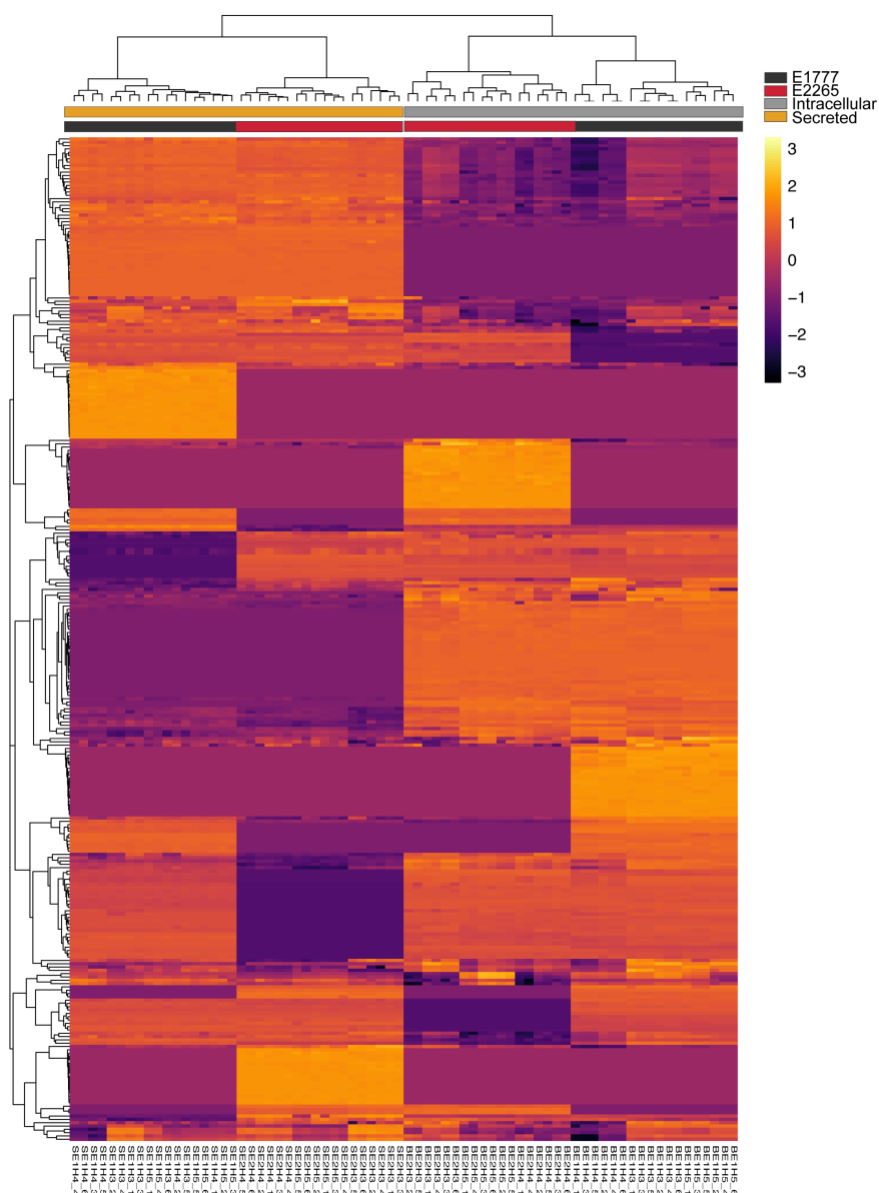
810

811   **Supplementary Figures**

812

813
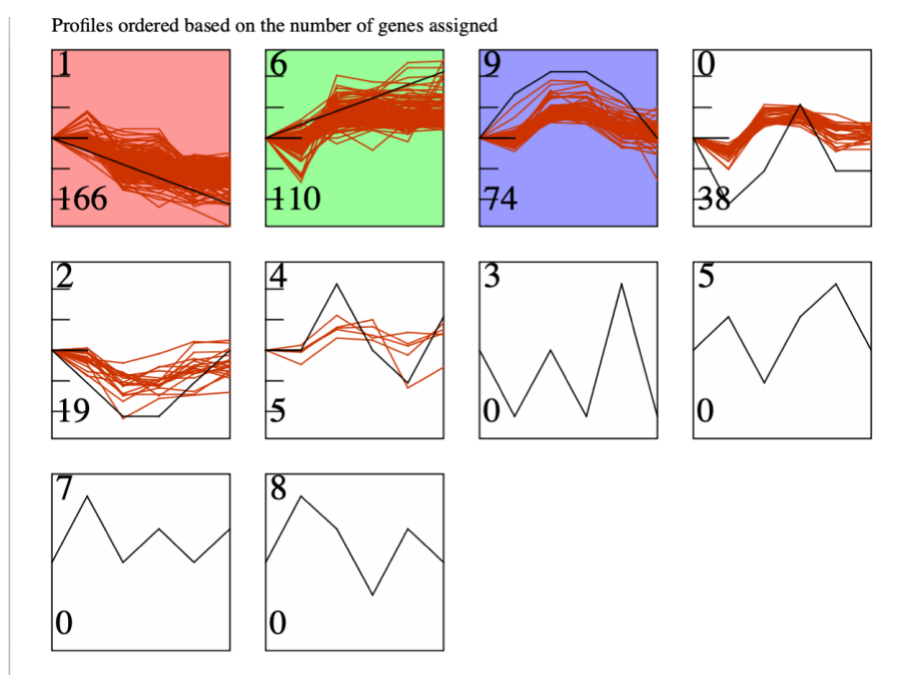
814   **S Figure 1.** Idenified gene expression patterns by STEM. The profile number
815   on the top left corner of each profile box was assigned by STEM and the
816   number on the bottom left represents the number of genes included in the
817   cluster. Clusters with a *p*-value >0.05 were colored.

818

819
820   **S Figure 2**. Heatmap representation of the abundance of 288 intracellular
821   and secreted metabolites detected in E2265 and E1777.
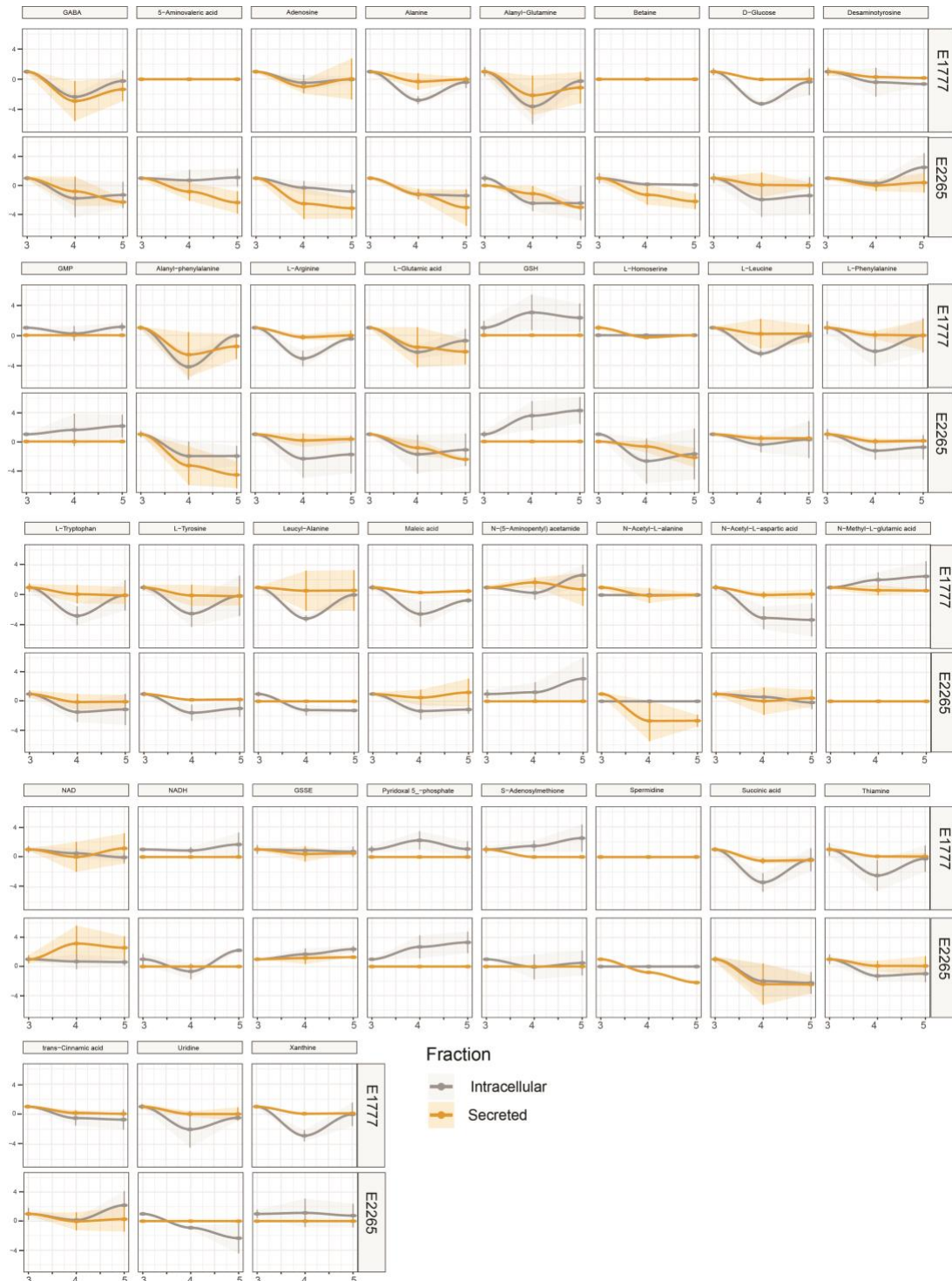
S Figure 3. Data of the concentration of all significant metabolites are represented in the serial charts. The metabolite concentration is adjusted to 3 h, and the data is presented in fold-change±SD.